

Chapter 9

Sensitivity of South American Tropical Climate to Last Glacial Maximum Boundary Conditions: Focus on Teleconnections with Tropics and Extratropics

Myriam Khodri, Masa Kageyama, and Didier M. Roche

Abstract We explore how the moist deep convection over the Amazonian region responds to glacial forcings compared to the pre-industrial climate and how this change might interact with the meridional shift of rainfall over Nordeste, Pacific and Atlantic tropical Oceans. The objective is to assess and investigate the individual contributions of greenhouse gases concentration, ice sheet topography and/or albedo on the hydrological changes over tropical South America and their links to the Hadley and Walker circulations. We employ coupled ocean-atmosphere simulations for the Last Glacial Maximum and sensitivity experiments for each Last Glacial Maximum forcing. We show that the Last Glacial Maximum reduced greenhouse gases alone can explain the observed rainfall changes over tropical South America through the induced increase in tropical and northern extra-tropical dry static stability and altered Hadley circulation. Furthermore, we show that the topography of the North American ice sheet reinforces the equatorward shift of the descending branch of the Hadley cell leading to stronger subsidence and drying over the northern tropics. However, we show that the Laurentide ice sheet has also a significant influence on the simulated enhanced rainfall over Nordeste and Southeastern Brazil via the eastward shift of the Walker circulation, with a mechanism analogous to the atmospheric thermodynamical response to El-Niño conditions.

Keywords Last Glacial Maximum · Teleconnections · South America · Hadley cell · Walker circulation · Inter Tropical Convergence Zone · Ocean atmosphere general circulation model

9.1 Introduction

To date, results obtained from paleoclimate proxies in the Tropics throughout the last glacial, deglacial and Holocene periods have largely been interpreted either in

M. Khodri (✉)

Institut de Recherche pour le Développement, IPSL/LOCEAN (CNRS, IRD, UPMC, MNHN),
Boîte 100, 4 place Jussieu, 75252 Paris, France
e-mail: myriam.khodri@ird.fr

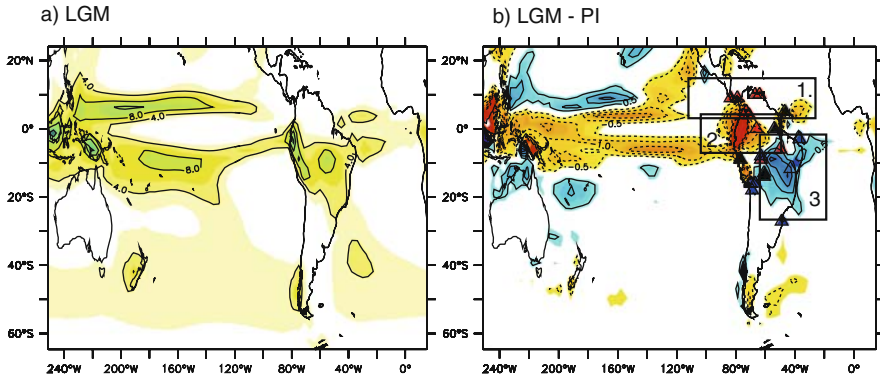


Fig. 9.1 Simulated precipitation during the Last Glacial Maximum by the IPSL-CM4 model and land records of hydrologic change over South America. **(a)** The background map shows Last Glacial Maximum December-January-February-March (DJFM) mean precipitation. Contour interval (CI) is 4 millimeters per day. **(b)** The background map shows Last Glacial Maximum precipitation changes respectively to pre-industrial (PI) conditions during DJFM. CI is 0.5 mm per day. *Blue shading* indicates positive values. *Red symbols* indicate more arid conditions during the Last Glacial Maximum, *black symbols* indicate a hiatus and *blue symbols* more humid conditions compared to present day (Data compilation after Koutavas and Lynch-Stieglitz 2004, see their Fig. 12-3 and Anhof et al. 2006; The speleothem record in Nordeste and Southeastern Brazil by Cruz et al. 2007 and Wang et al. 2006 are added to the previously cited compilations). Included sites are: Cariaco Basin (Peterson et al. 2000); Laguna el Pinal, Columbia (Behling and Hooghiemstra 1999); Lagoa Pata, Lagoa Gragao, Lagoa Verde (Colinvaux et al. 1996; Santos et al. 2001; Bush et al. 2004); Maicuru (Colinvaux and De Oliveira 2001); Carajas (Absy et al. 1991; Siffedine et al. 2001); Katira (Van der Hammen and Absy 1994); Noel Kempff Laguna Bella Vista (Mayle et al. 2000); Lake Valencia, Venezuela (Leyden 1985); El Valle Lake, Panama (Bush 2002); Lake Fuquene, Colombia (van Geel and van der Hammen 1973); Huascarán, Peru (Thompson et al. 1995); Sajama, Bolivi (Thompson et al. 1998); Illimani, Bolivia (Ramirez et al. 2003); Lake Titicaca, Bolivia (Baker et al. 2001); Lake Pata, Brazil (Colinvaux et al. 1996); ODP 932, Amazon Fan (Haberle and Maslin 1999); GeoB 3912 (Arz et al. 1998); Northeast Brazil (Wang et al. 2004); Southeast Brazil (Cruz et al. 2007)

terms of ENSO-like patterns or as changes in intensity and mean position of the Intertropical Convergence Zone (ITCZ) (e.g. Stott et al. 2002, 2004; Lea et al. 2003; Peterson et al. 2000; Koutavas et al. 2002; Koutavas and Lynch-Stieglitz 2003). For South America (SA) during the Last Glacial Maximum (LGM), 21 000 years Before Present (21 ky, BP) proxy data suggests a picture (Fig. 9.1b, symbols) with: (1) a drier tendency of the northern part of the continent and Central America, (2) a persistence of vegetation in the Amazon Basin, and (3) increased rainfall over southern tropics including the Nordeste, south east Brazil and the Altiplano of Bolivia. Given that the climate of the northern part of SA is affected mostly by the seasonal northward migration of the ITCZ, the LGM hydrology inferred from continental data has been interpreted as a southward shift of the ITCZ on annual mean (Koutavas and Lynch-Stieglitz 2004). Along the same line, Wang et al. (2007), based on speleothem records for the last glacial period, interpret the out of phase relationship between paleorainfall variability in Brazil and Eastern China as a direct response to

the reduced Atlantic meridional overturning circulation (AMOC) and its impact on the ITCZ position.

The seasonal cycle and amplitude of insolation received at the top of the atmosphere at the LGM is close to the present day one. The main LGM forcings are extensive land ice sheets over North America and Eurasia (Peltier 2004) and a reduced atmospheric concentration of greenhouse gases (GHG), notably of the atmospheric CO₂, which decreases by about 80 ppm (Flückiger et al. 1999; Dalenbach et al. 2000; Monnin et al. 2001). Both forcings and feedbacks within the climate system influenced and maintained the LGM climate. Changes in vegetation types might have also played a significant role through their influence on soil moisture variations, land surface albedo and evapo-transpiration (e.g. Kubatzki and Claussen 1998; Levis et al. 1999; Wyputta and McAvaney 2001).

Previous modelling studies have helped quantifying the impact of the land ice sheet and GHG forcings and their feedbacks on the LGM climate. Using atmospheric general circulation models (AGCMs) forced with the CLIMAP proxy-based reconstructions for LGM sea surface temperatures (SSTs), Hansen et al. (1984) have shown that land ice sheets and sea-ice albedo account for most of the LGM cooling. Coupling an AGCM to a slab ocean, other sensitivity studies has quantified the impact of each forcing on the simulated global cooling, revealing in most cases a strong influence of GHG on a global scale while land ice sheets lead to a cooling more restricted to the Northern Hemisphere (e.g. Manabe and Broccoli 1985). On the contrary, Hewitt and Mitchell (1997) relate most of the LGM global cooling to the topography and albedo of the land ice sheets while Felzer et al. (1998) argue for a combination between GHG and land ice influences. More recently, with a coupled ocean atmosphere GCM model (OAGCM), Kim (2004) evaluates that even though the bulk of global SST cooling is indeed due to reduced GHG, a larger cooling in the Northern Hemisphere occurs as response to either GHG and land ice sheets. The OAGCM results show greater cooling in the Northern Hemisphere in response to decreased Atlantic Meridional Overturning (AMOC) and ocean current heat exchange between both hemispheres.

According to tropical proxy data, such LGM global cooling correlates indeed with a reduced thermohaline circulation and with a drier rainy season in many tropical and monsoon regions between approximately 30°N and 5°N while wetter conditions develop in the southern tropics including northeastern Brazil (Nordeste). Chiang et al. (2003), based on paleoclimate observations and using an atmospheric climate model coupled to slab ocean suggest that the present-day “meridional mode” (labelled after Servain et al. 1999) of atmosphere-ocean variability in the tropical Atlantic is a potentially useful model for understanding these paleoclimate changes. The modern “meridional mode” corresponds to an anomalous meridional SST gradient across the equator, a displacement of the ITCZ and cross-equatorial flow toward the warmer hemisphere. The use of the “meridional mode” to explain LGM ITCZ mean position is largely based on the postulate that the dominant modern mode of tropical Atlantic ITCZ variability on inter annual-decadal timescales can link the climates of the tropical and North Atlantic. The marine-ITCZ, a tropical ocean-wide belt of atmospheric intense moist convection nowadays bears a year-round

Northern Hemisphere bias. It is located at the confluence of the northern and southern trades that sustain the rising branch of Hadley cell, is strongly linked to the South American Monsoon System and to the tropical seasonal emergence of cold equatorial SSTs (cold tongues) in the Atlantic and Pacific oceans. In the modern climate, very small interannual changes in tropical Atlantic SSTs (as small as 1°K) linked to NAO or ENSO external forcings explain part of the important ITCZ interannual to decadal variability observed in this ocean. Chiang et al. (2003), Chiang and Bitz (2005, referred herein as CB05) and Broccoli et al. 2006, using AGCMs coupled to a slab ocean, have shown that the Atlantic ITCZ response to LGM boundary forcings is analogous to the present day meridional mode with a southward displacement of the ITCZ. CB05 show that the North Atlantic cooling primarily promoted by the land ice sheets, with a negligible effect of reduced GHG, induces an asymmetric reorganisation of the Hadley circulation, a transfer of humidity toward the Southern Hemisphere through modified equatorial SST gradient and trans-equatorial winds.

Cruz et al. (cf. Chapter 2, this volume), based on this “ITCZ model”, argue that the links between the weakening of the East Asian summer Monsoons and the in-phase increased precipitation over Nordeste and in southern Brazil could be initiated by the cooling of North Atlantic Ocean. The authors relate such a cooling either to changes in the AMOC or to the “meridional mode”-like response to LGM forcings in the tropical Atlantic. Even though the “ITCZ model” might indeed provide some elements of explanation for the southward shift of the marine-ITCZ during the LGM, previous modelling results are limited by the absence of a fully interactive ocean and by a missing consistent mechanism for inland precipitation. Over SA, the northern trade winds that feed the monsoons are also strongly linked to moist deep convection processes over the Amazon basin, which could respond on its own right to the LGM forcings. The present day monsoon and ITCZ systems may be related and sometimes vary in pace over certain areas. However, their controlling factors are different and the mechanisms of their variability are also different (cf. Chapter 8, this volume). These aspects are directly of concern for paleoclimate issues since most recently published papers documenting past tropical climate changes tend to confuse the ITCZ dynamics and the monsoon itself.

Using 5 different AGCMs coupled to fully interactive oceans from the PMIP2 data-base (<http://pmip2.psce.ipsp.f2>, Braconnot et al. 2007), Khodri et al. (2009) have shown that the processes responsible for the LGM South American hydrological changes are independent from their Atlantic Ocean-ITCZ counterpart. In the 5 OAGCMs simulations, an intensification of the Hadley Cell and an equatorward shift of its northern boundary occur, caused by an increased northern hemisphere static stability. A narrower Hadley cell forms at the LGM characterized by a descending northern branch between 10°N and the equator. Such a subsidence explains most of the drying over northern tropical SA (region 1 in Fig. 9.1). This finding contrasts with the “meridional-mode” mechanism found by CB05 with a slab ocean, since in coupled models, the Hadley Cell response does not necessarily rely on a trans-equatorial SST gradient, winds and moisture fluxes. In southern tropical SA (region 2, Fig. 9.1), the drying tendency over the Amazon basin is shown

to be rather due to a strengthening and eastward shift of the Walker circulation. The eastward shift of the Walker circulation appears to be forced by the little cooling in Southeast Central (SEC) Pacific, as compared to the West Pacific Warm Pool (WPWP), reminiscent to an “El-Niño like” pattern. Increased precipitation over the Nordeste and southeastern Brazil (region 3, Fig. 9.1) is then favored since both regions are out of reach of the stabilizing effects of the Walker and Hadley components of the tropical circulation and are located right next to moisture sources (namely the Amazon basin and the South Atlantic) needed to trigger moist convection. The robustness of these physical processes across all models seems to be confirmed by available data over land and over the Pacific Ocean. Over the tropical ocean, recent proxy estimates indeed indicate a relatively uniform cooling of about $1.7 \pm 1^\circ\text{C}$ across the tropical oceans (with no trans-equatorial gradient in the Atlantic), while SEC Pacific shows little or no cooling at LGM as compared to modern times (Otto-Bliesner et al. 2009; MARGO Project Members 2009).

Numerous processes could affect the strength and extent of the Hadley cell and Walker circulation during LGM, such as the changes in the topography and/or albedo of the ice sheets and reduced GHG. We cannot exclude either a specific and more direct response of the moist deep convection over SA to the global mean cooling during the LGM. This chapter builds upon a previous modelling study (Khodri et al. 2009), by using one of the fully coupled PMIP2 OAGCMs used to simulate the LGM climate. The objective is to assess and investigate the individual contributions of GHG concentration, ice sheet topography and/or albedo on the hydrological changes over tropical SA and links to the Hadley and Walker circulations. Here after, we show that the LGM reduced greenhouse gases forcing alone can explain the observed rainfall changes over tropical SA through the induced increase in tropical and northern extra-tropical dry static stability and altered Hadley cell. Furthermore, we show that the topography of Laurentide land ice sheet reinforces the equatorward shift of the northern bound of the Hadley cell leading to stronger subsidence and drying over northern tropics. Finally, we will also show that the Laurentide ice sheet has a significant influence on the simulated enhanced rainfall over Nordeste and Southeastern Brazil via the eastward shift of the Walker circulation.

Section 9.2 describes the model and its applicability to our problem. Section 9.3 describes the results for the full LGM climate. Section 9.4 explores the impact of individual LGM forcings on the Hadley cell, the Walker circulation and tropical moist convection. Discussion and conclusions are given in Section 9.4.

9.2 Model Description and Simulated Thermo-Dynamical Structure of the Atmosphere

9.2.1 The Model and Experimental Set Up

The model simulations analyzed in this chapter rely on the IPSL-CM4-V1 coupled ocean-atmosphere general circulation model developed at the Institut Pierre

Table 9.1 Boundary conditions for the Pre-industrial (PI) and Last Glacial Maximum (LGM) climates

	Ice sheets	Coastlines	CO ₂ (ppmv)	CH ₄ (ppbv)	NO ₂ (ppbv)	Eccentricity	Obliquity (°)	Angular precession (°)
PI	Modern	Modern	280	760	270	0.0167724	23.446	102.04
LGM (21 ky)	ICE-5G	ICE-5G	185	350	200	0.018994	22.949	114.42

Simon Laplace (Marti et al. 2005) that has been extensively used for present, future and past climate studies. It is part of PMIP2 model simulation database for the LGM and preindustrial (PI) conditions (<http://www-lsce.cea.fr/pmip2/>, Braconnot et al. 2007). In the PMIP2 framework, all model simulations have the same boundary conditions for both the LGM and PI climates (see Table 9.1). Details of the experimental protocols are given in Braconnot et al. (2007). In the coupled ocean-atmosphere experiments analyzed in the present chapter the vegetation is fixed and prescribed to the present day distribution. The control simulation corresponds to a pre-industrial climate with atmospheric trace gases concentrations of 1750 A.D. and the 1950 orbital configuration (the 1750 and 1950 insolation difference is negligible). The LGM boundary conditions correspond to the topography and ice albedo from the ICE-5G data set developed by Peltier (2004). Changes in coastlines due to the decreased sea level induced by the large amount of frozen ice in continental ice-sheets are also taken into account leading to additional land in the Tropics (in the Indonesian Archipelago and between Australia and New Guinea). The specified greenhouse gas concentrations were inferred from the Greenland and Antarctic ice core records (Fluckiger et al. 1999; Dallenbach et al. 2000; Monnin et al. 2001) showing reduced concentrations of atmospheric carbon dioxide (CO₂), methane (CH₄), and nitrous oxide (NO₂) (Table 9.1). Otto-Bliesner et al. (2006a) have shown that LGM decreased greenhouse gases relative to PI resulted in a radiative forcing of the troposphere of -2.8 W m^{-2} . The orbital configuration of 21 ky BP is close to the present day.

In addition to the full LGM climate simulation, four additional sensitivity experiments have been performed (Kageyama et al. in prep), starting from PI conditions and adding in each simulation either: (1) the LGM reduced concentrations of atmospheric GHG (referred herein as LGMGHG); (2) the LGM land ice albedo and topography but with pre-industrial GHG concentrations (referred herein as LANDICE); (3) the topography of the ice sheet only without the corresponding albedo forcing (referred herein as ICETOPO); and (4) the albedo of the land ice distributed over the area of the ice sheet mask but without its topography (referred herein as ICEALB). Table 9.2 summarizes the configurations used in each sensitivity experiment. Each simulation is 500 years long and the last 50 years are used to compute the mean seasonal cycle. To explore the models skills related to the tropical climate, we choose to only examine quantities being useful diagnostics for

Table 9.2 Configuration of the sensitivity experiments to the Last Glacial Maximum forcing parameters

	LGMGHG	LANDICE	ICETOPO	ICEALB
Greenhouse gases	Last Glacial Maximum	PI	PI	PI
Topography	PI	ICE-5G	ICE-5G	PI
Albedo	PI	ICE-5G	PI	ICE-5G

tropical moist deep convection regions. In the following, we present the simulated large-scale features of tropical precipitations and the thermo-dynamical structure (static stability, stream function, 200 mb velocity potential and divergent winds) of the atmosphere during the southern tropic rainy season (austral summer: December-January-February-March, DJFM). Vimeux and Khodri (2009), have indeed shown that it is the DJFM precipitation changes in the Tropics that imprint the simulated LGM annual response over SA and surrounding tropical oceans.

9.2.2 Simulated Pre-industrial (PI) Climate

We remind the readers that the model configuration is for pre-industrial conditions, which might induce some discrepancies when compared to present day observations. We do not present the results for the full seasonal cycle for the sake of simplicity. The PI model simulation exhibits a realistic seasonal cycle of precipitation and of sea-surface temperature (not shown). Figure 9.2 shows that the overall large-scale characteristics of the tropical precipitation for PI climate are well depicted when compared to the CMAP precipitation data set (Xie and Arkin 1997). Over SA the model does a good job in representing the observed geographical and amplitude characteristics of the austral summer South American Monsoon with precipitation spreading from the northern tropical Atlantic Ocean, into the Amazonian Basin and prolonged to the southeast by the South Atlantic Convergence Zone (SACZ). We note however, a strong positive precipitation bias on the Pacific coast but the overall characteristics of the South American Monsoon are well depicted.

Figure 9.3a and b display the vertical structure of the atmosphere static stability in DJFM for ERA40 and as simulated for PI conditions respectively. Static stability is one of the most fundamental quantities describing the state of the atmosphere. It derives from the vertical equivalent potential temperature (θ) structure of the atmosphere and determines the buoyancy force in the vertical. The vertical buoyancy force can be formalized as follow:

$$d\omega/dt = gz(\gamma - \gamma_d)/T_A$$

where ω is the vertical motion, γ corresponds to the environmental lapse-rate, γ_d to the adiabatic lapse-rate and T_A the environmental atmospheric temperature.

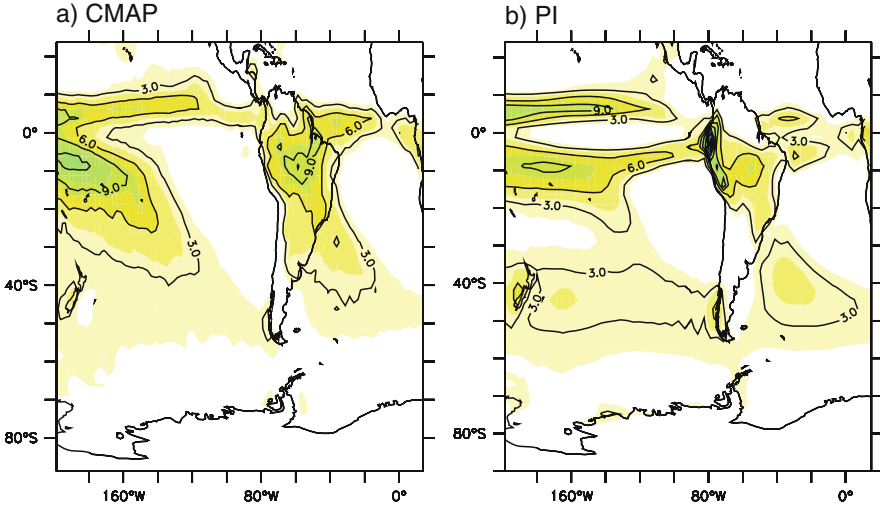


Fig. 9.2 Mean precipitation in DJFM. Colour shading interval is 2 mm per day. *Solid line* interval is 3 mm per day. (a) CMAP precipitation data set. (b) Model simulated precipitation for pre-industrial conditions

The atmosphere is stable ($d\omega/dt < 0$) when $\gamma < \gamma_d$, neutral when $\gamma = \gamma_d$ ($d\omega/dt = 0$) and unstable ($d\omega/dt > 0$) when $\gamma > \gamma_d$. Using the hydrostatic approximation ($dp/dz = -\rho g$, with ρ being the air density and dp/dz the vertical pressure gradient), the static stability converts to:

$$d\omega/dt = g(\rho_a - \rho)/\rho$$

ρ_a is the density of the environment, ρ the density of the moving air parcel and $g(\rho_a - \rho)$ the vertical buoyancy force.

The vertical structure of equivalent potential temperature (θ), plotted on Fig. 9.3a and b, can then be used to estimate the atmospheric static stability against deep convection. The potential temperature of a parcel of air, θ , corresponds to the temperature that the parcel would attain if it were displaced to the surface pressure reference level P_{00} (~ 1000 mb) in a reversible adiabatic process (i.e. no exchange of heat with the environment atmosphere). It is defined as follow:

$$\theta = T(P_{00}/P)^k, \text{ with } k = Rd/C_p,$$

where Rd corresponds to the gas constant for dry air and C_p to the specific heat of air at constant pressure. θ implicitly takes into account the effects of compressibility of the air and it is used to remove the cooling (warming) effects associated to adiabatic processes (compression for dry air). θ therefore allows a direct comparison of air parcels temperature at various levels in the atmosphere. Within tropical moist deep convective regions the moist adiabat assumes that a local heating of an air mass

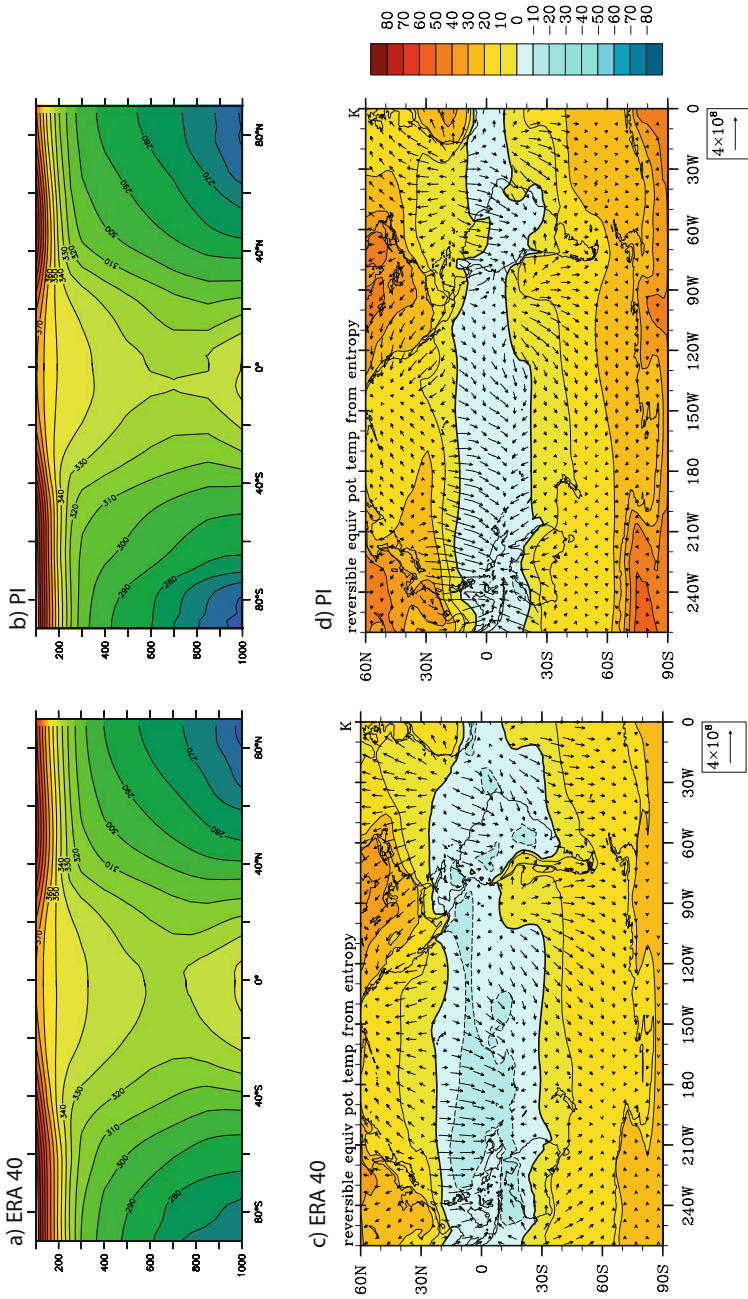


Fig. 9.3 (a) Vertical structure of the equivalent potential temperature (θ) in DJFM for (a) ERA40 and (b) for simulated pre-industrial (PI) conditions. CI is 10 K. Vertical coordinate is pressure in millibar (mb). The *lower panels* show the bulk static stability defined as the difference of θ between the upper troposphere (400 mb) and the surface (1000 mb) for (c) ERA40 and (d) for simulated pre-industrial (PI) conditions. The *blue shading* indicates negative values and corresponds to regions of minimum stability. Vertically integrated latent heat flux divergence is overlaid as vectors. Unit is $\text{J m}^{-1} \text{s}^{-1}$. The reference vector is indicated on the *lower part* of each graph

can destabilize it if it becomes warmer than the surrounding air at the same altitude. Being warmer it expands, which reduces its density ($\rho < \rho_a$), which in turn increases its buoyancy force, so it keeps rising ($d\omega/dt > 0$). When it rises it cools adiabatically (i.e. no exchange of heat between a parcel of ascending air and the environment) at the dry rate ($-10^\circ\text{C}/\text{km}$) while the environment cools at the normal rate ($-6^\circ\text{C}/\text{km}$). So the air parcel becomes colder until $\rho = \rho_a$ and the buoyancy ($d\omega/dt$) decreases. But if the dew point temperature is reached during the rising, the cooling lapse rate slows down to the wet adiabat lapse rate, which is smaller than the environment lapse rate and the energy released during condensation is used to warm the parcel. The atmosphere remains unstable and the air continues to rise and remains buoyant. At one point, at a certain altitude, the rising air temperature catches up with the temperature of stable air, it loses its extra buoyancy, ceases to rise further and the atmosphere becomes stable.

So the static stability can be expressed by $d\theta/dz$, with an unstable atmosphere when $d\theta/dz < 0$, a stable atmosphere when $d\theta/dz > 0$, and a neutral atmosphere with respect to deep convection when $d\theta/dz = 0$. As shown on Fig. 9.3 (upper panels), the uniform vertical profile of θ within the tropics between 30°S and 30°N illustrates that the temperature structure in the tropics is approximately given by the moist adiabat (Xu and Emanuel 1989). Within tropical moist deep convection areas, the warm sea surface temperature promotes strong surface buoyancy explaining the quasi standardization of the vertical temperature profile of θ between 30°S – 30°N (dry air following the dry lapse rate), which in fact reflects the surface θ . In addition, as shown in Fig. 9.3a, b, the latitudinal and vertical structure of θ show that moist convection that occurs over tropical warm waters determine upper tropospheric temperatures over mid-latitudes and is important in establishing the static stability from tropical to extra-tropical latitudes.

On Fig. 9.3c, the bulk static stability, defined as the difference of θ between the upper troposphere (400 mb) and the surface (1000 mb) shows that the Tropics bear minimum stability ($d\theta/dz < 0$, minimum vertical gradient of θ) while extra-tropical latitudes are much more stable against convection ($d\theta/dz > 0$, maximum vertical gradient of θ). Interestingly, the model does a fairly good job in representing the thermal structure of the atmosphere even though it underestimates the latitudinal extent of tropical moist deep convective region (blue area, Fig. 9.3d). The model bears a much narrower tropical belt of unstable atmosphere relatively to observations. This difference is probably due to the overall cold SSTs bias of 1 K in the tropics simulated with PI boundary conditions when compared to modern day (Otto-Bliesner et al. 2009, their Fig. 9.2). The vertically integrated divergent latent heat transport is overlaid as vectors on Fig. 9.3c and d. The low-level latent heat divergence from eastern pacific upwelling regions towards the WPWP, illustrating the low level flow of the atmospheric Walker Circulation is well captured in pattern while its strength is underestimated.

The zonally-averaged atmospheric streamfunction displayed on Fig. 9.4a and b features the DJFM Hadley circulation for NCEP and the PI run respectively. Positive (negative) values represent a (counter) clockwise mass flux circulation. The Hadley circulation is constrained by the requirement that diabatic heating in the Tropics

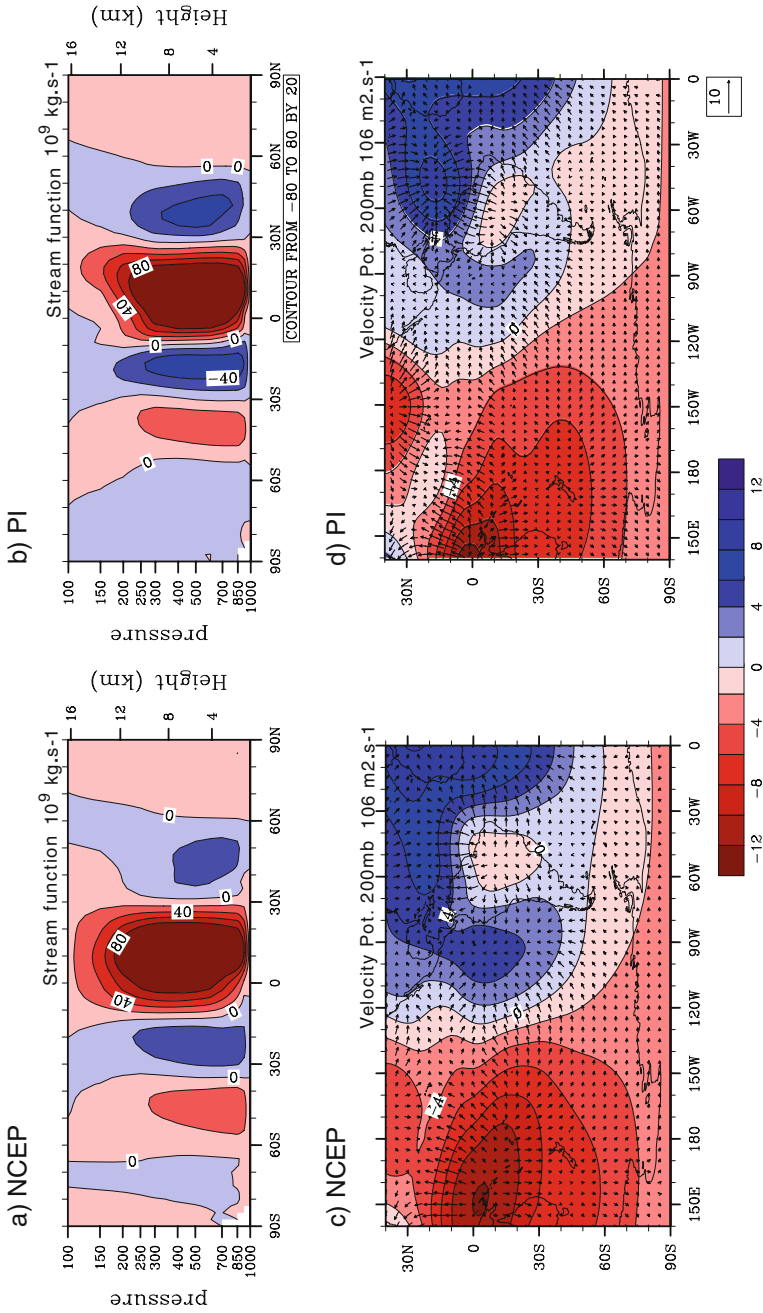


Fig. 9.4 Stream function (10^9 kg s^{-1}) in DJFM for (a) NCEP reanalyses and (b) for the simulated pre-industrial (PI) conditions. Red (blue) shading indicates positive clockwise (negative counter clockwise) circulation. Vertical coordinate is pressure in millibar (mb). (c) and (d) 200 mb velocity potential ($10^6 \text{ m}^2 \text{ s}^{-1}$) and divergent winds (m s^{-1}) overlaid as vectors for NCEP reanalyses and for the simulated pre-industrial (PI) conditions. The reference vector is indicated on the lower part of each graph. Convergence corresponds to positive (blue shading) velocity potential

sustaining the divergent flow in the upper troposphere balances the cooling leading to subsidence in subtropics. The model simulation for PI conditions does a fairly good job in representing the meridional extent and strength of the Hadley cell even though the vertical component of the divergence within the Tropics is weaker than observed. Along the same lines, the 200 mb velocity potential and divergent wind vectors on the lower panels of Fig. 9.4, showing the upper tropospheric large-scale motion, depict the links between the Hadley and Walker circulations and tropical convective regions. The Hadley circulation follows the strong divergent flux from the convective Amazonian basin and WPWP toward the subtropical latitudes of both hemispheres, while divergent winds from the WPWP toward the eastern Pacific illustrates the upper flow of the atmospheric Walker Circulation. The lower panels of Fig. 9.4 confirm the underestimation of the extent and intensity of tropical moist deep convective regions (seen with the bulk of dry static stability, Figs. 9.3c, d) by the IPSL model. Over SA and the WPWP, the area of upper divergent flow (pink and red shading) is smaller than observed.

To sum up, the large-scale features of the thermo-dynamical structure of the PI tropical atmosphere simulated by the model, including its dry static stability, the Walker and Hadley (upper and lower) tropical circulations are underestimated when compared to observations and reanalyses of the present features. This overall weaker tropical circulation could be related to the cold bias in the simulation due to PI conditions.

9.3 Response of Tropical South American Climate to Last Glacial Maximum Forcings

In this section we present the changes in surface temperature gradient, precipitation, dry static stability, zonal and meridional atmospheric circulations in response to the applied LGM forcings. For conciseness, the processes behind the simulated SST changes are not fully developed here and will be the subject of an upcoming paper. Only the impact of the applied forcings on the tropical climate of SA will be discussed.

9.3.1 The Last Glacial Maximum

The simulated surface annual SST changes simulated for the LGM by the IPSL model shows an uniform tropical (15°S–15°N) cooling of about 2.3°K, which compares relatively well to the MARGO estimation of $1.7 \pm 1^\circ\text{K}$ (MARGO project members 2009; Otto-Bliesner et al. 2009). Concerning the regional patterns, Otto-Bliesner et al. (2009) have shown that the inter basin and intra basin SST cooling gradients are underestimated by coupled models when compared to MARGO estimations. Here, we have chosen to focus on the sign of changes in surface temperature gradient rather than the net values in order to get a better understanding of

the processes controlling the zonally-asymmetric Walker circulation in the tropical Pacific. Figure 9.5a displays the DJFM surface temperature gradient difference in response to the applied LGM forcings (see caption for details). According to the MARGO proxy data, the SST has greater LGM cooling in the eastern Pacific cold tongue than in the WPWP, which suggests a stronger zonal SST gradient. Observations also indicate that there is little or no cooling over the Pacific subtropical gyres, in the SEC and Northeast Pacific (MARGO project members 2009). For the full LGM simulated climate, on Fig. 9.5a, smaller cooling in the WPWP is found compared to the eastern Pacific cold tongue. Likewise, SEC and North Eastern Central

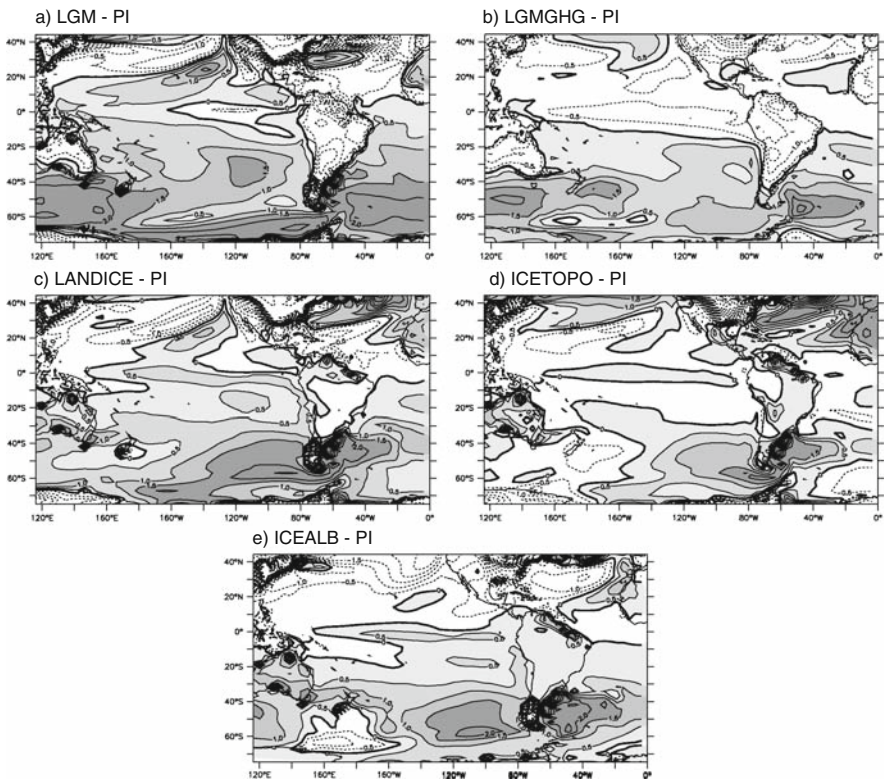


Fig. 9.5 Changes in surface temperature gradient respectively to the pre-industrial simulation. The surface temperature gradient was computed by removing linearly the averaged global surface temperature to each corresponding surface temperature field. The removal of the global average facilitates the comparison of the regional pattern between the sensitivity experiments and PI conditions. This shows the DJFM mean difference between the (a) LGM (GHG, orbital, and land ice forcing) and the PI run; (b) LGMGHG (GHG only) and the PI run; (c) LANDICE (land ice forcing only) and the PI run; (d) ICETOPO (land ice topography only) and the PI run; (e) ICEALB (land ice albedo only) and the PI run. CI is 0.5 °K and regions above the thick zero line contour are shaded

Pacific bear the least cooling as compared to the abovementioned regions. Reasoning in terms of gradient, the simulated DJFM pattern over the Pacific Ocean might suggest an overall agreement with the MARGO data compilation, even if the amplitude of the changes is weaker. Noteworthy over the Atlantic, the simulated trans-equatorial SST gradient with stronger cooling in the Northern Hemisphere is inconsistent with the MARGO data compilation. This is due to the fact that the PI climate has a relatively weak thermohaline overturning (~ 12 sverdrup, Sv) while the LGM has a strong one (~ 15 Sv).

Figure 9.6 shows the LGM response in atmospheric static stability (upper panels) and circulation changes (lower panels) simulated by the IPSL model respectively to PI conditions. On Fig. 9.6a, the changes in the vertical structure of the equivalent potential temperature (θ), reveal a robust increase in LGM dry static stability, with the lower tropospheric cooling outpacing the upper troposphere by about 2 K on a global average. The globally cooler and drier LGM climate promotes a contraction of the atmosphere, which becomes denser as evidenced by the lower tropopause

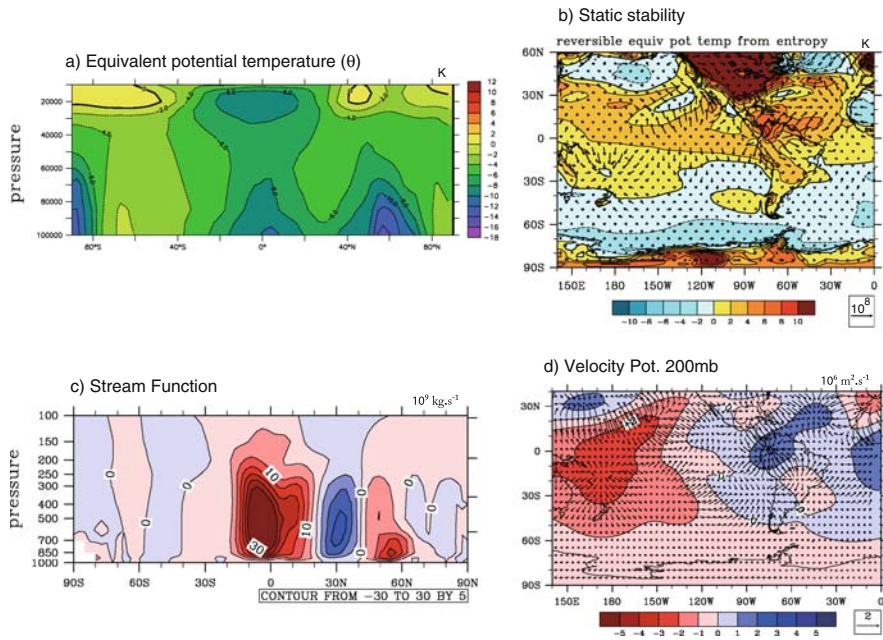


Fig. 9.6 Changes in dry static stability and atmospheric circulation given LGM boundary conditions. This shows the DJFM mean difference between the LGM (GHG, orbital, and land ice forcing) and the PI run. **(a)** Vertical structure of the equivalent potential temperature (θ) (CI 2°K); **(b)** Bulk static stability (CI 2°K and the thick line is the zero contour) and vertically integrated latent heat flux divergence overlaid as vectors ($\text{J m}^{-1} \text{s}^{-1}$, the reference vector is given on the panel); **(c)** Streamfunction (*red shading* indicates positive values); **(d)** 200 mb velocity potential (CI is $1.10^6 \text{m}^2 \text{s}^{-1}$) and divergent winds (m s^{-1} , reference vector is given on the panel) overlaid as vectors

Table 9.3 Simulated tropical (15°S–15°N) precipitation, (mm per day) and surface temperature (°k) changes in each simulation respectively to PI conditions

		LGM-PI	LGMGHG-PI	LANDICE-PI	ICETOPO-PI	ICEALB-PI
Precipitation	AN	-0.39	-0.3	0	0.09	0
	DJFM	-0.38	-0.33	0	0.1	0
Surface Temperature	AN	-2.3	-2.2	0.57	1.4	0.2
	DJFM	-2.2	-2.2	0.32	1.4	0.28

height (positive values on Fig. 9.6a). Over tropical latitudes between 15°S and 15°N, this results in a damping of the convective heating of the upper troposphere, explaining the slight tropical mean decrease in precipitation especially over tropical Pacific and northern SA (Fig. 9.1). Despite the slight net precipitation decrease on average over tropical latitudes (Table 9.3), rainfall increases substantially over Nordeste and Southeastern Brazil.

It is worth noting however that a larger thermal stratification occurs over northern extra-tropics (+3.5 °K) as compared to the southern tropics (+0.8 °K) probably because of the presence of large land ice cover in the Northern Hemisphere. An intensification of the Hadley Cell and an equatorward shift of its northern boundary are simulated (Fig. 9.6c). This narrower Hadley cell feeds upon the core of baroclinic eddies developing south of the Laurentide Ice sheet. The resulting stronger subsidence between 10°N and the equator (Fig. 9.6d) then provides a dynamical feedback amplifying the drying tendency seen over northern tropical SA (region 1 in Fig. 9.1). Such an increased Hadley cell circulation seems to be a direct consequence of the increased dry static stability over extra tropical latitudes, which pushes the baroclinic instability zone and the outer limit of the Hadley cell equatorward. This result confirms that tropical circulation may indeed depend on extratropical climate since the boundary condition for the Hadley circulation is constrained by the requirement that diabatic heating in the tropics balances cooling in subtropics. Such extratropic-tropic dependence is stronger at the LGM due to the stronger perturbation of northern extra tropical thermal and dynamical equilibrium.

As expected from the reinforced tropical Pacific zonal SST gradient, a strengthening of the Walker circulation is simulated, as shown by the changes in the 200 mb velocity potential (Fig. 9.6d). The smaller SST cooling over SEC Pacific as compared to the WPWP induces also a positive anomaly in diabatic heating for the atmosphere and is responsible for an anomalous divergence east of 120°W (Fig. 9.6d, pink shading). As a result stronger divergent mass flux from SEC Pacific and stronger subsidence over most of the Amazon basin (Fig. 9.6d, blue shading) are simulated consistently with an eastward extension of the Walker circulation. Overall, the model shows a tendency towards a more “El Niño-like” state in terms of the perturbation of thermal structure of the tropical atmosphere. This is shown by the meridional mean of tropical equivalent potential temperature displayed on Fig. 9.7a,b. The equivalent potential temperature changes simulated at LGM are reminiscent to the tropospheric temperature anomaly in response to an “El Niño-

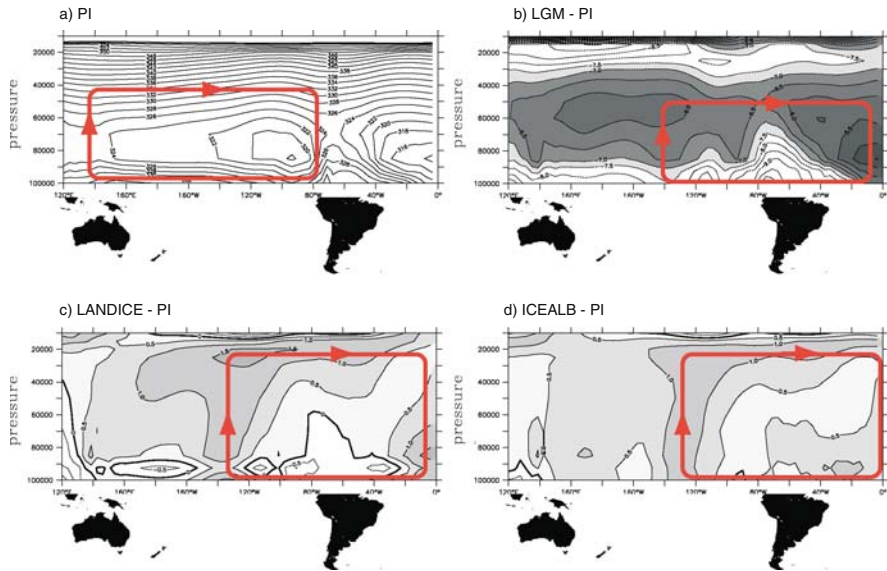


Fig. 9.7 Changes in the tropical (15°S – 15°N) meridional mean of dry static stability. This shows the vertical structure of the tropical zonal mean of equivalent potential temperature (θ) in DJFM for (a) for the PI run. CI is 2°K ; (b) the difference between the LGM (GHG, orbital, and land ice forcing only) and the PI run. Regions above the -7.5°K contour are shaded; (c) the difference between the LANDICE (land ice forcing only) and the PI run; CI is 2°K ; (d) the difference between the ICEALB (land ice albedo only) and the PI run. CI is 0.5°K and regions above the thick zero line contour are shaded. Vertical coordinate is pressure in Pascal (Pa)

like” state, which consists in a widespread warming of upper troposphere compared to lower level, spreading outward from the central Pacific (Wallace et al. 1998; Chiang and Sobel 2002; Su and Neelin 2002). However such an anomalous upper tropospheric warming differs from a canonical “El-Niño-like” state since here it is due to warmer conditions in the SEC Pacific as compared the WPWP. This tropical-tropical teleconnection provides a second mechanism by which the atmospheric column is stabilized (both thermally and dynamically) against deep convection over equatorial SA. As moisture accumulates in the boundary layer over the Amazon to balance the reduced local moist deep convection, a transfer of humidity occurs from the Amazon basin toward the Nordeste and Southeast Brazil. This is well illustrated by the changes in the bulk of static stability and moisture divergence displayed on Fig. 9.6b. The Amazonian moisture is removed by the low-level flow and transferred into the Nordeste and southeastern Brazil where moist convection can occur.

In the following sections, the role played by each LGM boundary condition on the abovementioned physical processes (damping of tropical convective heating, strengthening and contraction of the Hadley cell, strengthening and eastward extension of the Walker circulation) are investigated.

9.3.2 Sensitivity to Last Glacial Maximum Reduced Greenhouse Gases

Figure 9.8a displays the DJFM precipitation changes simulated by the LGMGHG run compared to the PI simulation. While the tropical average is negative (Table 9.3), there is a substantial positive precipitation anomaly occurring along the border of the Amazonian convection zone including the Nordeste and South East Brazil. These features are similar to the full Last Glacial Maximum case (Fig. 9.1) although with a weaker amplitude. The simulated tropical cooling reaches 2.2°K with reduced GHG, which is nearly equal to the full LGM tropical cooling (Table 9.3).

This suggests that the decreased absorption of infrared radiation induced by lower GHG concentration is mostly responsible for the direct thermo-dynamical adjustment of tropical moist deep convection, as shown on Fig. 9.9a (to be compared with Fig. 9.6a). Indeed the tropical cooling due to reduced GHG, equivalent to the full LGM case, results in a direct atmospheric column drying (low-level specific humidity reduced by about 15%) following the Clausius-Clapeyron relationship and leading to increased tropical dry static stability (Figs. 9.9a, b). Such a tropical atmospheric stabilisation also implies a reduction in water vapor low-level convergence especially over tropical Pacific, which provides amplification for the drying (Fig. 9.9b).

However across the Tropics, the bulk dry static stability anomalies are relatively constant, with positive anomalies spreading between 30°N and 30°S , which therefore do not, on their own, yield insight into the mechanisms for the strong spatial structure in the precipitation signal over tropical SA. Interestingly, reduced

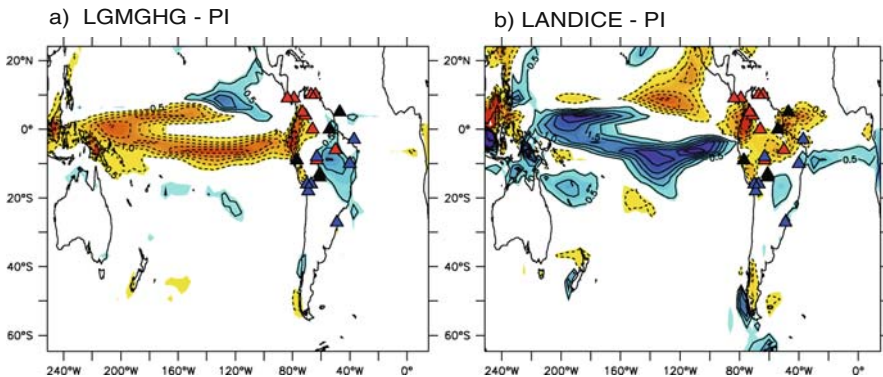


Fig. 9.8 Simulated precipitation changes and land records (symbols) of hydrologic change over South America (see caption of Fig. 9.1). This shows the DJFM mean difference between the (a) LGMGHG (GHG only) and the PI run; (b) LANDICE (land ice forcing only) and the PI run. CI is 0.5 mm per day. Blue shading indicates positive values. Red symbols indicate more arid conditions during the Last Glacial Maximum, black symbols indicate a hiatus and blue symbols more humid conditions compared to present day

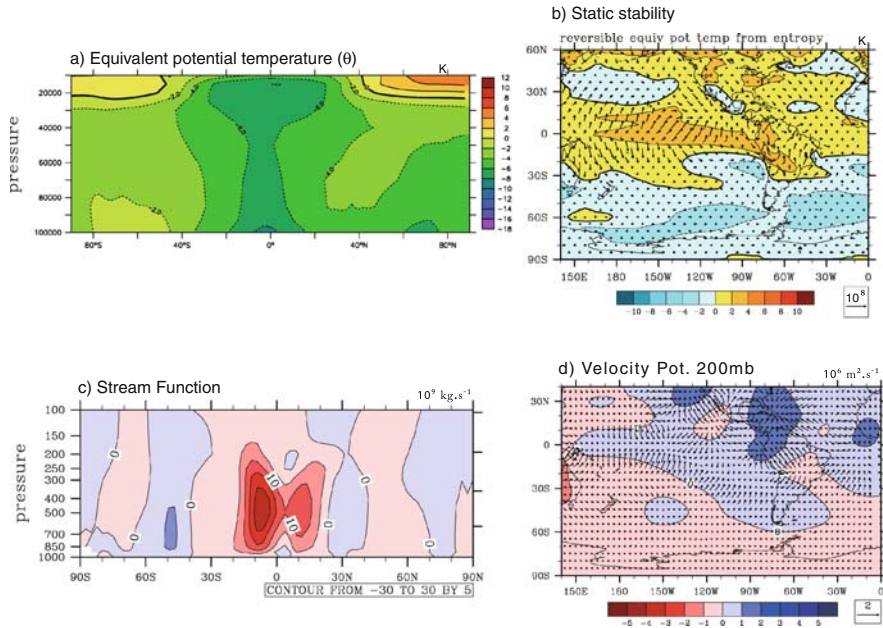


Fig. 9.9 Same as Fig. 9.6 but given LGMGHG (GHG only) boundary conditions

GHG also leads to a stronger cooling of Northern Hemisphere compared to the Southern Hemisphere, due to the presence of more land masses which on average respond more importantly to the radiative cooling than the southern oceans (Fig. 9.5b; Laine et al. 2009). As a result, the static stability increases more in the Northern Hemisphere as compared to the Southern Hemisphere, which pushes both the baroclinic instability zone and hence the northern boundary of the Hadley cell southward as in the full LGM case (Fig. 9.9c). A robust strengthening of the Hadley cell and subsidence occurring over equatorial and northern SA (Fig. 9.9d, blue shading) provides therefore an amplifying feedback mechanism (in addition to the direct impact of the cooling) for reduced precipitation. These features resemble the mechanism presented by CB05 and Broccoli et al. (2006), relying only on the asymmetric temperature changes between both hemispheres to explain the net southward shift of the Atlantic ITCZ. However in the full LGM and LGMGHG simulation, no southward shift of the Atlantic ITCZ and trans-equatorial moisture transport are reproduced. Instead analysis of the boundary layer moisture budget over the Amazon basin reveals that the accumulation of moisture in the Amazonian boundary layer due to decreased local deep convection is moved by the divergent flow (overlaid latent heat divergent transport on Fig. 9.9b) into the Nordeste and southeast Brazilian coast, where moist instability actually occurs.

The above mentioned physical processes due to reduced GHG alone (radiative tropical cooling and damping of convective mass fluxes, strengthening but limited

expansion of the Hadley cell, transfer of moisture and rainfall from the Amazon basin toward the Nordeste) account for most of the LGM changes over the equatorial Pacific and northern SA. However, the somewhat less pronounced enhanced rainfall over southeast Brazil compared to the full LGM case could be due to the absence of the Walker circulation feedback. This is well illustrated by the overall uniform cooling across the tropical Pacific and the absence of eastward shift of the Walker circulation (Fig. 9.9d). A similar analysis for the simulation taking into account the Northern Hemisphere LGM land ice only as a boundary condition, shows that the mechanism of teleconnection with the central Pacific applies essentially to southern tropical latitudes of SA.

9.3.3 Sensitivity to Last Glacial Maximum Land Ice

On Fig. 9.8b the DJFM precipitation changes simulated in the LANDICE sensitivity experiment reveals a balance between an increased precipitation over the tropical Pacific and a drying tendency over most of tropical SA (Table 9.3). This result confirms that net decreased tropical precipitation during LGM is mostly due to the reduced GHG and induced radiative cooling. Similarly to the full LGM and LGMGHG case however, a hemispheric asymmetry of static stability and limited expansion of the Hadley cell (Fig. 9.10a–c) is simulated. The land ice forcing acts to cool the northern lower troposphere while forcing a southeastward shift of the subtropical jet and western ocean boundary currents (i.e the Atlantic Gulf Stream and

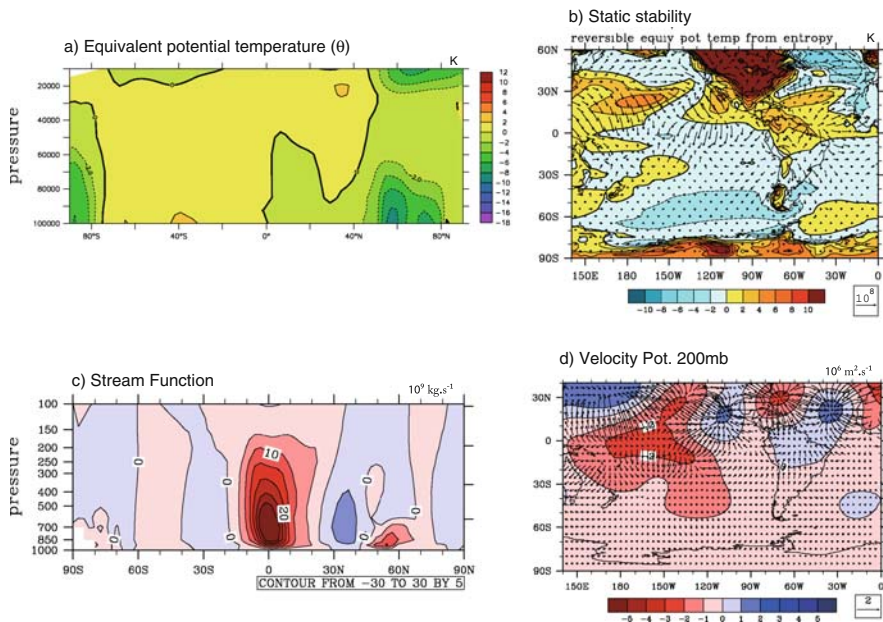


Fig. 9.10 Same as Fig. 9.6 but given LANDICE (land ice forcing only) boundary conditions

the Pacific Kuroshio, not shown) explaining the warmer SST over the subtropical gyres of both hemispheres (Fig. 9.5c). The impact on the bulk dry static stability anomalies across the Tropics and on the Hadley cell subsidence over northern tropical SA is nevertheless much weaker (Fig 9.10b, d) than for the full LGM and LGMGHG cases and is confined north of the equator.

Precipitation changes for southern tropical SA (Fig. 9.8b) appears to be linked to the teleconnection with the central Pacific. Despite the reduced zonal SST gradient and intensity of the Walker circulation, the warmer SEC Pacific sustains an upper tropospheric increase of θ which reaches 1.5°K over SA (Fig. 9.7c). The resulting eastward shift of the Walker circulation (Fig. 9.10d), amplified atmospheric thermal stratification over southern tropical SA and reduced moisture convergence (Fig. 9.10b), all induce a damping in moist deep convection including most of the Nordeste and southeastern Brazil. Interestingly adding up LGMGHG and LANDICE results (not shown) reveals that the precipitation field obtained is close to the full LGM, which suggests a linear response to both forcings. Reduced GHG and land ice at LGM both contribute to reduced precipitation over northern tropical SA via the Hadley cell thermodynamical adjustments, but the net southeastward shift of the precipitation towards Nordeste and southeast Brazil is amplified when involving “El-Niño like” teleconnection with SEC Pacific and gradient in the boundary layer moisture.

Accordingly when separating the topography from the albedo forcing of land ice, both forcings lead to similar precipitation responses. Increased rainfall over the tropical Pacific is in both cases compensated by drying over tropical SA (Fig. 9.11, Table 9.3). Adding the anomalies due to individual ice albedo and topography forcings does not reproduce the LANDICE precipitation changes (not shown) suggesting a non linear combination of their effects. Indeed while the higher topography barrier in the ICETOPO experiment induces a local thermal stratification over the northern extratropics and a southward shift of the jet stream and of the northern boundary of the Hadley cell, the resulting subsidence over northern SA is weaker

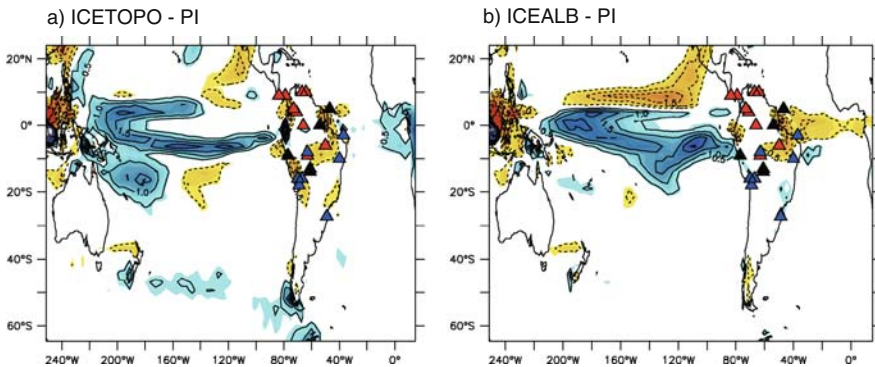


Fig. 9.11 Same as Fig. 9.8 but given (a) ICETOPO (land ice topography only) and (b) ICEALB (land ice albedo only) boundary conditions

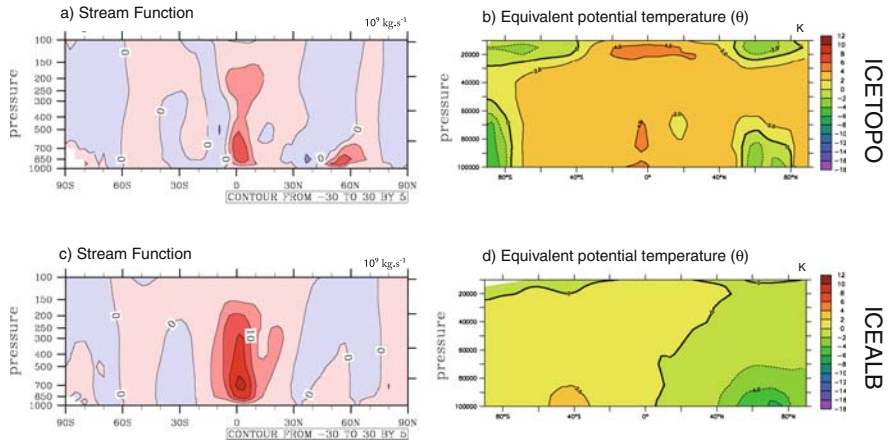


Fig. 9.12 Changes in mean streamfunction and vertical structure of the equivalent potential temperature (θ) in ICETOPO (land ice topography only, upper panels) and ICEALB (land ice albedo only, lower panels) boundary conditions. This shows the DJFM mean difference to the PI run. In (b) and (d) CI is 2°K and the thick line is the zero contour. For the streamfunction, the red shading indicates positive values

than in LANDICE (Fig. 9.12a, b). This suggests that the dynamical teleconnection alone with the topography of the Laurentide Ice sheet through its influence on the position of the outer boundary of the Hadley cell can explain only part of the drying over northern SA. In the absence of global cooling, the transfer of moist deep convection preferentially occurs towards the tropical Pacific Ocean (as in LANDICE), where abundant moisture supply is not a barrier for convection and even tends to be enhanced by the increased moisture convergence (not shown).

A most interesting result is that in response to the sole ice albedo forcing (unlike in LANDICE or ICETOPO), there is a robust poleward expansion of the Hadley circulation (Fig. 9.12c) despite the inter-hemispheric SST asymmetry and strong surface temperature gradient on the southern limit of the Laurentide Ice sheet (Fig. 9.5e). The ice albedo alone then sustains a strong horizontal gradient in northern static stability, which, in the absence of topographic barrier, pushes the baroclinic instability zone and the northern limit of the Hadley cell poleward (Fig. 9.12c, d). Therefore, in the ICEALB experiment, the Hadley cell subsidence mechanism cannot explain the drying tendency over northern SA. The warm SST in the SEC Pacific however leads to the positive upper tropospheric θ anomaly over tropical SA (Fig. 9.7d), as seen in the LANDICE case. This result confirms that tropospheric warming spreading out from the Pacific and eastward extension of the Walker circulation is the essential mechanism for the drying over equatorial America and is due to the ice albedo.

These results show that the mechanisms of climate change over South America can be broken down between a response to (1) the direct effect on tropical deep

convection of global cooling and associated drying due to reduced GHG (Clausius-Clapeyron relationship); (2) the effect of increased extra-tropical static stability on the Hadley Cell and stronger subsidence over northern tropics due to both reduced GHG and the topography of the ice-sheets; and (3) the influence of SEC Pacific SST positive anomaly, probably due to the land ice albedo, on the strengthening and eastward extension of the Walker circulation.

9.4 Summary and Conclusion

Proxy data over South America for the LGM has been interpreted as a southward shift of the ITCZ, which has been so far linked to a trans-equatorial gradient in the Atlantic Ocean, analogous to the modern day “meridional-mode” mechanism (Chiang et al. 2003; Chiang and Bitz 2005). Here we have explored alternative mechanisms, related to the direct impact of the LGM global cooling and changes in the dry static stability on tropical moist deep convection. We have used a coupled ocean-atmosphere model capable of capturing the thermodynamical structure of the atmosphere and the tropical component of the Hadley and Walker circulations. In each experiment, we have applied either all the LGM forcings, or the individual contributions of greenhouse gases (GHG) concentrations, ice sheet topography and/or albedo to explore the hydrological response over tropical latitudes with a focus on South America.

The dominant forcing for the LGM tropical temperature and precipitation changes is found to be due to the reduced GHG, which explains almost entirely the simulated tropical cooling and drying. The LGM GHG is also responsible for a stronger cooling in the Northern Hemisphere, inducing a stronger overall northern tropical overturning atmospheric circulation. Such a stronger northern component of the tropical Hadley cell appears to be caused by increased extra-tropical static stability. Stronger subsidence over northern tropic then produces an amplification of the northern tropical drying initially due to the direct cooling effect. The boundary layer moisture accumulated in the Amazon basin is then transferred by the low level circulation towards the Nordeste where rainfall increases. The land ice sheet is also able to promote the Hadley cell feedback mostly via the topographic effect on the extra-tropical dry static stability and on the position of the subtropical jets. Our results therefore suggest that the communication between the extra tropics and the tropics is tighter during LGM and does not necessarily rely on the “meridional-mode” mechanism. The Hadley cell response is constrained by the requirement that diabatic heating in the Tropics balances cooling in subtropics. We show that such extratropic-tropic dependence is stronger at the LGM because of the stronger perturbation of northern extra tropical thermal and dynamical equilibrium due to both reduced GHG and land ice sheets. Such a mechanism is potentially useful to explain northern tropical drying and seems to be confirmed by available proxy data. Furthermore the MARGO data compilation indeed suggests a uniform latitudinal cooling across tropical latitudes of the Atlantic Ocean, therefore inconsistent with a “meridional-mode” mechanism.

The role of the ice albedo appears to be nontrivial since, in the absence of the land ice topographic barrier, its influence results in poleward extension of the Hadley cell through the stronger horizontal gradient in static stability. As the topography and albedo influences on the simulated changes are not linear and even lead to opposite responses of the Hadley cell, it is difficult to interpret their respective role in the total land ice forcing. This result sheds some light on the processes that could be at work during the last deglaciation and on the possibility of a threshold from which the land ice sheet would rather favour a northward expansion of the Hadley cell and non-linear shift in the position of tropical drying. Such processes could also be particularly relevant for warm stadials of Dansgaard-Oeschger events or even for the Bølling-Allerød. Paleoproxy records show that warm events over Greenland correspond to a northward shift of the ITCZ as recorded for example by the Cariaco basin sediments north to Venezuela (Peterson et al. 2000). To the extent that Cariaco records can be translated into Amazon convection variations, we suggest that this link could be related to the direct ice sheet impact on the atmosphere. Such an extra-tropical tropical link could work as an additional process to the usually incriminated impact of changes in overturning circulation (Rahmstorf 2002) on the trans-equatorial ITCZ shift. The land ice directly influences the atmospheric circulation in the mid-latitudes and tropics and because of the antagonist effects of its topography and albedo could lead to nonlinear atmospheric circulation responses when it collapses.

We also show that the overall tropical Pacific circulation response to land ice consists in a substantial thermo-dynamical stabilisation of the tropical atmosphere over the Amazon basin, resulting in reduced precipitation. The upper troposphere warming over tropical latitudes spreading out from the South East Central (SEC) Pacific, reminiscent of the one occurring during an El-Niño event, seems to be due to the albedo component alone. We conclude with a cautionary remark related to the realism of the simulated SST changes in the LGM simulations. We reasoned in terms of gradient in order to decipher the processes, evaluate the response of the zonally-asymmetric Walker circulation and meridional tropical overturning associated with the Hadley cell. We have shown that even though the SST gradient across the Tropics and subtropical Pacific are reminiscent of those observed in MARGO data compilations, the comparison for the Atlantic Ocean is however inconsistent. Sensitivity experiments using an atmospheric only GCM directly forced by the MARGO SST for each season will help in evaluating the realism of processes evidenced here. We did not take into account the biosphere-atmosphere interactions but such interactions would probably have strong implications for the South American Monsoon response to glacial boundary conditions. For this reason biosphere-atmosphere interactions need to be considered in future work.

References

- Absy ML, Cleef A, Fournier M, Martin L, Servant M, Sifeddine A, Ferreira da Silva M, Soubiès F, Suguio K, Turcq B, Van der Hammen T (1991) Mise en évidence de quatre phases d'ouverture de la forêt amazonienne dans le sud-est de l'Amazonie au cours des 60000 dernières années.

- Première comparaison avec d'autres régions tropicales. *Comptes Rendus de l'Académie des Sciences*. Paris 312:673–678
- Anhuf D, Ledru MP, Behling H, Da Cruz FW Jr, Cordeiro RC, Van der Hammen T, Karmann I, Marengo JA, De Oliveira PE, Pessenda L, Siffedine A, Albuquerque AL, Da Silva Dias PL (2006) Paleo-environmental change in Amazonian and African rainforest during the Last Glacial Maximum. *Palaeogeogr Palaeoclimatol Palaeoecol* 239:510–527
- Arz HW, Pätzold J, Wefer G (1998) Correlated millennial-scale changes in surface hydrography and terrigenous sediment yield inferred from last-glacial marine deposits off northeastern Brazil. *Quat Res* 50:157–166
- Baker PA, Seltzer GO, Fritz SC, Dunbar RB, Grove MJ, Tapia PM, Cross SL, Rowe HD, Broda JP (2001) The history of South American tropical precipitation for the past 25,000 years. *Science* 291:640–643
- Behling H, Hooghiemstra H (1999) Environmental history of the Colombian savannas of the Llanos Orientales since the Last Glacial Maximum from lake records El Pinal and Carimagua. *J Paleolimnol* 21:461–476
- Bush MB (2002) On the interpretation of fossil Poaceae pollen in the lowland humid neotropics. *Palaeogeogr Palaeoclimatol Palaeoecol* 177:5–17
- Braconnot P, Otto-Bliesner BL, Harrison SP et al (2007) Results of PMIP2 coupled simulations of the mid-holocene and last glacial maximum—part 1: experiments and large-scale features. *Clim Past* 3:261–277
- Broccoli AJ, Dahl KA, Stouffer RJ (2006) Response of the ITCZ to Northern Hemisphere cooling. *Geophys Res Lett*, DOI 10.1029/2005GL024546
- Bush MB, De Oliveira PE, Colinvaux PA, Miller MC, Moreno JE (2004) Amazonian paleoecological histories: one hill, three watersheds. *Palaeo* 214:459–475
- Chiang JCH, Sobel AH (2002) Tropical tropospheric temperature variations caused by ENSO and their influence on the remote tropical climate. *J Clim* 15:2616–2631
- Chiang JCH, Biasutti M, Battisti DS (2003) Sensitivity of the Atlantic Intertropical Convergence Zone to Last Glacial Maximum boundary conditions. *Paleoceanography*. DOI 10.1029/2003PA000916
- Chiang JCH, Bitz CM (2005) Influence of high latitude ice cover on the marine Intertropical Convergence Zone. *Clim Dyn*. doi: 10.1007/s00382-005-0040-5
- Colinvaux PA, De Oliveira PE, Moreno JE, Miller MC, Bush MB (1996) A long pollen record from lowland Amazonia: forest and cooling in glacial times. *Science* 274:85–88
- Colinvaux PA, De Oliveira PE (2001) Palaeoecology and climate of the Amazon basin during the last glacial cycle. *J Quat Sci* 15:347–356
- Cruz FW, Burns SJ, Jercinovic M, Karmann I, Sharp WD, Vuille M (2007) Evidence of rainfall variations in southern Brazil from trace element ratios (Mg/Ca and Sr/Ca) in a Late Pleistocene stalagmite. *Geochim Cosmochim Acta* 71:2250–2263
- Dallenbach A, Blunier T, Flückiger J, Stauffer B, Chappellaz J, Raynaud D (2000) Changes in the atmospheric CH₄ gradient between Greenland and Antarctica during the last glacial and the transition to the holocene. *Geophys Res Lett* 27:1005–1008
- Felzer B, Webb T, Oglesby RJ (1998) The impact of ice sheets, CO₂, and orbital insolation on late quaternary climates: sensitivity experiments with a general circulation model. *Quat Sci Rev* 17:507–534
- Flückiger J, Dallenbach A, Blunier T, Stauffer B, Stocker TF, Raynaud D, Barnola JM (1999) Variations in atmospheric N₂O concentration during abrupt climatic changes. *Science* 285:227–230
- Haberle SG, Maslin MA (1999) Late Quaternary vegetation and climate change in the Amazon basin based on a 50,000 year pollen record from the Amazon fan, ODP site 932. *Quat Res* 51:27–38
- Hansen J, Lacis A, Rind D, Russell G, Stone P, Fung I, Ruedy R, Lerner J (1984) Climate sensitivity: analysis of feedback mechanisms. In: Hansen J, Takahashi T (eds) *Climate processes and climate sensitivity*. *Geophys Mono* 29, Am Geophys Union, Washington, DC, 130–163

- Hewitt CD, Mitchell JF (1997) Radiative forcing and response of a GCM to ice age boundary conditions: cloud feedback and climate sensitivity. *Clim Dyn* 13:821–834
- Kageyama M, Braconnot P, Grégoire L, Khodri M, Lañé A, Roche D (2009) Role of CO₂, land ice topography and albedo in the Last Glacial Maximum climate. In prep
- Khodri M, Kageyama M, Ramstein G, Braconnot P, Turcq B (2009) Mechanism of climate change over South America during Last Glacial Maximum – Part 1: a multiple coupled ocean-atmosphere model study. Submitted to *J Geophys Res*
- Kim SJ (2004) The effect of atmospheric CO₂ and ice sheet topography on Last Glacial Maximum climate. *Climate Dyn* 22:639–651, doi: 10.1007/s00382-004-0412-2
- Koutavas A, Lynch-Stieglitz J, Marchitto TM Jr, Sachs JP (2002) El Niño-like pattern in ice age tropical Pacific sea surface temperature. *Science* 297:226–230
- Koutavas A, Lynch-Stieglitz J (2003) Glacial-interglacial dynamics of the eastern equatorial–Pacific cold tongue–Intertropical Convergence Zone system reconstructed from oxygen isotope records. *Paleoceanography* 18. doi: 10.1029/2003PA000894
- Koutavas A, Lynch-Stieglitz J (2004) Variability of the marine ITCZ over the Eastern Pacific during the past 30,000 years: Regional perspective and global context. In: Diaz HF, Bradley RS (eds) *The Hadley circulation: present, past, and future*. Kluwer Academic Press, Dordrecht
- Kubatzki C, Claussen M (1998) Simulation of the global bio-geophysical interactions during the Last Glacial Maximum. *Clim Dyn* 14:461–471
- Lea DW, Pak DK, Peterson LC, Hughen KA (2003) Synchronicity of tropical and high-latitude Atlantic temperatures over the last glacial termination. *Science* 301 1362–1364
- Lañé A, Kageyama M, Braconnot P, Alkama R (2009) Impact of greenhouse gas concentration changes on the surface energetics in the IPSL-CM4 model: regional warming patterns, land/sea warming ratio, glacial/interglacial differences accepted *J Clim*
- Levis S, Foley JA, Pollard D (1999) CO₂, climate, and vegetation feedbacks at the Last Glacial Maximum. *J Geophys Res* 104:191–198
- Leyden B (1985) Late Quaternary aridity and Holocene moisture fluctuations in the Lake Valencia Basin, Venezuela. *Ecology* 66:1279–1295
- Manabe S, Broccoli AJ (1985) The influence of continental ice sheets on the climate of an ice age. *J Geophys Res* 90:2167–2190
- Marti O, Braconnot P, Bellier J, Benschila R, Bony S, Brockmann P, Cadule P, Caubel A, Denvil S, Dufresne JL, Fairhead L, Filiberti MA, Foujols MA, Fichefet T, Friedlingstein P, Goosse H, Grandpeix JY, Hourdin F, Krinner G, Lévy C, Madec G, Musat I, deNoblet N, Polcher J, Talandier C (2005) The New IPSL Climate System Model: IPSL-CM4, Note du Pôle de Modélisation, n 26, ISSN 1288-1619
- MARGO Project Members (2009) Constraints on the magnitude and patterns of ocean cooling at the last glacial maximum. *Nat Geosci*. doi: 10.1038/NGEO0411
- Mayle FE, Burbridge R, Killeen TJ (2000) Millennial-scale dynamics of southern Amazonian rainforest. *Science* 290:2291–2294
- Monnin E, Indermuhle A, Dallenbach A, Fluckiger J, Stauffer B, Stocker TF, Raynaud D, Barnola JM (2001) Atmospheric CO₂ concentrations over the last glacial termination. *Science* 291:112–114 947
- Otto-Bliesner BL, Brady EC, Clauzet G, Tomas R, Levis S, Kothavala Z (2006a) Last glacial maximum and Holocene climate in CCSM3. *J Clim* 19:2526–2544
- Otto-Bliesner BL, Schneider R, Brady EC, Kucera M, Abe-Ouchi A, Bard E, Braconnot P, Crucifix M, Hewitt C, Kageyama M, Marti O, Paul A, Rosell-Mele A, Waelbroeck C, Weber SL, Weinelt M, Yu Y (2009) A comparison of PMIP2 model simulations and the MARGO proxy reconstruction for tropical sea surface temperatures at last glacial maximum. *Clim Dyn*. doi: 10.1007/s00382-008-0509-0
- Peterson LC, Haug GH, Hughen KA, Rohl U (2000) Rapid changes in the hydrologic cycle of the tropical Atlantic during the last glacial. *Science* 290:1947–1951
- Peltier WR (2004) Global glacial isostasy and the surface of the ice-age Earth: the ICE-5G(VM2) model and GRACE. *Annu Rev Earth Planet Sci* 32:111–149

- Rahmstorf S (2002) Ocean circulation and climate during the past 120,000 years. *Nature* 419: 207–214
- Ramirez E, Hoffmann G, Taupin JD, Francou B, Ribstein P, Caillon N, Ferron FA, Landais A, Petit JR, Pouyaud B, Schotterer U, Simoes JC, Stievenard M (2003) A new Andean deep ice core from Nevado Illimani, (6350 m), Bolivia. *Earth Planet Sci Letters* 212: 337–350
- Santos G, Cordeiro RC, Silva Filho EV, Turcq B, Fifield LK, Gomes PRS, Hausladen A, Siffeddine A (2001) Chronology of atmospheric mercury in Lagoa Da Pata basin, upper Rio Negro region of Brazilian Amazon. *Radiocarbon* 43(2):801–808
- Servain J, Wainer I, McCreary JP Jr, Dessier A (1999) Relationship between the equatorial and meridional modes of climatic variability in the tropical Atlantic. *Geophys Res Lett* 26: 485–488
- Siffeddine A, Martin L, Turcq B, Volkmer-Ribeiro C, Soubiès F, Campello Cordeiro R, Suguio K (2001) Variations of the Amazonian rainforest environment: a sedimentological record covering 30,000 years. *Palaeogeogr Palaeoclimatol Palaeoecol* 168:221–235
- Stott L, Poulson C, Lund S, Thunell R (2002) Super ENSO and global climate oscillations at millennial time scales. *Science* 297:222–226
- Stott L, Cannariato KG, Thunell R, Haug GH, Koutavas A, Lund S (2004) Decline of surface temperature and salinity in the western tropical Pacific Ocean in the Holocene epoch. *Nature* 431:56–59
- Su HS, Neelin JD (2002) Teleconnection mechanisms for tropical pacific descent anomalies during El Niño. *J Atmos Sci* 59:2694–2712
- Thompson LG, Mosley-Thompson E, Davis ME, Lin PN, Henderson KA, Cole-Dai J, Bolzan JF, Liu K (1995) Late glacial stage and Holocene tropical ice core records from Huascarán, Peru. *Science* 269:46–50
- Thompson LG, Davis ME, Mosley-Thompson E, Sowers TA, Henderson KA, Zagorodnov VS, Lin PN, Mikhalenko VN, Campen RK, Bolzan JF, Cole-Dai J, Francou B (1998) A 25,000-year tropical climate history from Bolivian ice cores. *Science* 282:1858–1864
- van Geel B, van der Hammen T (1973) Upper Quaternary vegetational and climatic sequence of the Fuquene area (Eastern Cordillera, Colombia). *Palaeogeogr Palaeoclimatol Palaeoecol* 14:9–55
- Van der Hammen T, Absy ML (1994) Amazonia during the last glacial. *Palaeo* 109: 247–261.
- Vimeux F, Khodri M (2009) Mechanism of climate change over South America during Last Glacial Maximum – Part 2: New insights to interpret the glacial-interglacial isotopic variation in Andean ice cores. Submitted to *J Geophys Res*
- Wallace JM, Rasmusson EM, Mitchell TP, Kousky VE, Sarachik ES, von Storch H (1998) On the structure and evolution of ENSO-related climate variability in the tropical Pacific: lessons from TOGA. *J Geophys Res* 103:14241–14260
- Wang X, Auler AS, Edwards RL, Cheng H, Cristalli PS, Smart PL, Richards DA, Shen C-C (2004) Wet periods in northeastern Brazil over the past 210 kyr linked to distant climate anomalies. *Nature* 432:740–743
- Wang X, Auler AS, Edwards RL, Cheng H, Ito E, Solheid M (2006) Interhemispheric anti-phasing of rainfall during the last glacial period. *Quat Sci Rev* 25:3391–3403
- Wang X, Edwards RL, Auler AS, Cheng H, Ito E (2007) Millennial-Scale interhemispheric asymmetry of low-latitude precipitation: Speleothem evidence and possible high-latitude forcing. *Geophys Monograph Series* 173:279–293
- Wyputta U, McAvaney BJ (2001) Influence of vegetation changes during the Last Glacial Maximum using the BMRC atmospheric general circulation model. *Clim Dyn* 17:923–932
- Xie PP, Arkin PA (1997) Global precipitation: a 17-year monthly analysis based on gauge observations, satellite estimates, and numerical model outputs. *Bull Am Meteorol Soc* 78: 2539–2558
- Xu KM, Emanuel KA (1989) Is the tropical atmosphere conditionally unstable? *Mon Wea Rev* 117:1471–1479